

Article

Climate Change Impacts on Drought-Flood Abrupt Alternation and Water Quality in the Hetao Area, China

Yuheng Yang¹, Baisha Weng^{1,*}, Wuxia Bi^{1,2} , Ting Xu¹ , Dengming Yan^{1,3} and Jun Ma^{1,4}

¹ State Key Laboratory of Simulation and Regulation of Water Cycle in River Basin, China Institute of Water Resources and Hydropower Research, Beijing 100038, China; 1109080115@cau.edu.cn (Y.Y.); biwuxia_1992@163.com (W.B.); xuting900515@163.com (T.X.); 201513408@mail.sdu.edu.cn (D.Y.); 201613332@mail.sdu.edu.cn (J.M.)

² College of Hydrology and Water Resources, Hohai University, Nanjing 210098, China

³ College of Environmental Science and Engineering, Donghua University, Shanghai 201620, China

⁴ School of Water Conservancy and Hydroelectric Power, Hebei University of Engineering, Handan 056021, China

* Correspondence: baishaweng@163.com; Tel.: +86-136-0598-2766

Received: 26 February 2019; Accepted: 21 March 2019; Published: 29 March 2019

Abstract: Drought-flood abrupt alternation (DFAA) is an extreme hydrological phenomenon caused by meteorological anomalies. To combat the climate change, the watershed integrated management model—Soil and Water Assessment Tool model (SWAT)—was used to simulate DFAA, total nitrogen (TN) and total phosphorus (TP) from 1961 to 2050, based on measured precipitation data in the Hetao area and the downscaled Representative Concentration Pathways (RCPs) climate scenarios. In the future, the increase in temperature and the increase in extreme precipitation will aggravate the pollution of water bodies. Results indicate that the risk of water quality exceeding the standard will increase when DFAA happens, and the risk of water quality exceeding the standard was the greatest in the case of drought-to-flood events. Results also indicate that, against the backdrop of increasing temperature and increasing precipitation in the future, the frequency of long-cycle and short-cycle drought-flood abrupt alternation index (LDFAI, SDFAI) in the Hetao area will continue to decrease, and the number of DFAA situations will decrease. However, the zone of high-frequency DFAA situations will move westward from the eastern Ulansuhai Nur Lake, continuing to pose a risk of water quality deterioration in that region. These results could provide a basis for flood control, drought resistance and pollution control in the Hetao and other areas.

Keywords: drought-flood abrupt alternation; temporal and spatial evolution; climate change; water quality; Copula function

1. Introduction

In 2018, the Intergovernmental Panel on Climate Change (IPCC) pointed out that the global average temperature has risen by nearly 1.5 °C, and it is predicted that it will increase by another 1.1–6.4 °C in 2100 [1,2]. The Fifth Assessment Report (AR5) of the IPCC stated that climate system warming is an undoubted fact [3]. Climate warming has not only directly affects extreme temperature fluctuations but also increases the frequency and intensity of extreme weather, such as, high temperature, droughts, rainstorms and floods, especially in areas sensitive and vulnerable to climate change [4–6].

DFAA is a type of extreme weather affected by climate change [7]. It refers to drought in a certain period of time and flooding in another period, an alternating occurrence of droughts and floods [8]. DFAA research increased in the 20th century. During this period, there were more extensive and

thorough researches on extreme droughts and floods, of their causes, their alternating occurrence and their co-occurrence. Vogel et al. [9] studied the weather sources of abnormal precipitation in St. Louis by the METROMEX network method. Trenberth et al. [10] studied the extreme drought in 1988 and the physical causes of the extreme flood in 1993 in the United States.

The relationship between atmospheric circulation anomalies and DFAA is also the focus of scholars [11]. Garnett et al. [12] conducted a statistical analysis of the effects of El Niño-Southern Oscillation (ENSO) and Indian monsoon droughts and floods on food production using global food production data. Hastenrath et al. [13] studied atmospheric circulation mechanism anomalies in the droughts and floods change in eastern Equatorial Africa from 2005 to 2008. Chinese researchers are concentrating on the middle and lower reaches of the Yangtze River where DFAA frequently occurs. Yang et al. [7] believed that the significant differences in water vapor transport flux and the atmospheric circulation field before and after DFAA are the main reasons for DFAA in the middle and lower reaches of the Yangtze River in 2011. Zhang et al. [14] revealed that in addition to climatic factors, land-water storage anomalies and the contradiction between the characteristics of easily occurring flood (drought) and insufficient flood drainage (drought control) ability are also major causes.

To analyze the law of DFAA, historical data was applied to study its occurrence, and evaluation indicators were used to predict the future DFAA characteristics [15,16]. In terms of the evaluation indicators, the precipitation-based summer LDFAI has been widely used in predicting the turn from drought to flood as well as the turn from flood-to-drought during flood season [17,18]. Wu et al. [19,20] analyzed the characteristics of DFAA in the summer of a normal monsoon year and predicted that the total precipitation during the co-occurrence of drought and flood, and DFAA in the summer in southern China tended to be normal. Mosavi et al. [21,22] used machine learning models and hybrid neuro-fuzzy algorithms to predict the likelihood of future floods and droughts. After predicting future drought and flooding results, the sensitivity of the results should be tested. Choubin, et al. [23] used multivariate discriminant analysis, classification and regression trees, and support vector machines to perform sensitivity tests on flood prediction results. In addition, the occurrence of drought and flood in the regions affected by global climate change and human activities has been increasingly frequent, and the possibility of DFAA continues to increase [24,25].

Currently, progress has been made in the study of DFAA, but the following problems remain for further study: (1) Due to the lack of study on DFAA with a long sequence scale, there is no distinct definition of its temporal and spatial scales. (2) Previous studies focused on historical DFAA, and there is a lack of estimation of the evolution law of DFAA in the future. (3) Previous studies have focused on the evolution law analysis of DFAA, single cause analysis or studies on its law evolution and coping mechanisms but have not been connected with water pollution to form a systematic research method for DFAA. Therefore, this study attempted to estimate the change characteristics of future DFAA in the Hetao area by using the Representative Concentration Pathways (RCPs) climate scenario, and to estimate the occurrence probability of water pollution in future DFAA scenarios by simulating future water quality changes in Hetao area. Moreover, the characteristics of DFAA in this area were studied to cope with emergencies caused by climate change in advance, further provided a scientific basis for drought and flood control as well as water pollution control in the Hetao area.

2. Materials and Methods

2.1. Study Area

The Hetao area is located in the southern part of Bayannaor City, Inner Mongolia Autonomous Region (Figure 1). The Hetao area has a complex spatial structure with an average elevation difference of less than 37 m. In addition, large-scale and long-term water resource development and other human activities in the irrigation area interfere with the canal system for irrigation and drainage. The annual precipitation is 50 to 250 mm, with large annual fluctuation. The precipitation in summer accounts for over 60% of the annual precipitation and that in spring only accounts for 10% to 20% [26].

The drought in spring is especially serious. Thus, DFAA typically occurs at the turn of spring to summer. The main river systems in the Hetao area are the Yellow River and Ulansuhai Nur Lake. Ulansuhai Nur Lake is the largest lake in the Hetao area, which is a part of the Yellow River [27]. Due to the large amount of agricultural wastewater discharge in the Hetao area, more than 90% of farmland irrigation (approximately 1.07×10^6 ha) water is discharged into Ulansuhai Nur Lake [27]. In addition, with the rapid development of local industries and population growth in recent years, industrial and domestic wastewater discharge has begun to exceed the standard [26]. As a result, the pollution load of TN and TP in the Ulansuhai Nur Lake area far exceeds the carrying capacity of the lake [28]. In summary, frequent DFAA in the Hetao area will lead to sudden water pollution in the Ulansuhai Nur Lake, thereby damaging the industrial and agricultural production and ecological environment in this region. Therefore, it is of both scientific and practical significance to study the characteristics and evolution of DFAA in the Hetao area and to further study the water quality of the Ulansuhai Nur Lake.

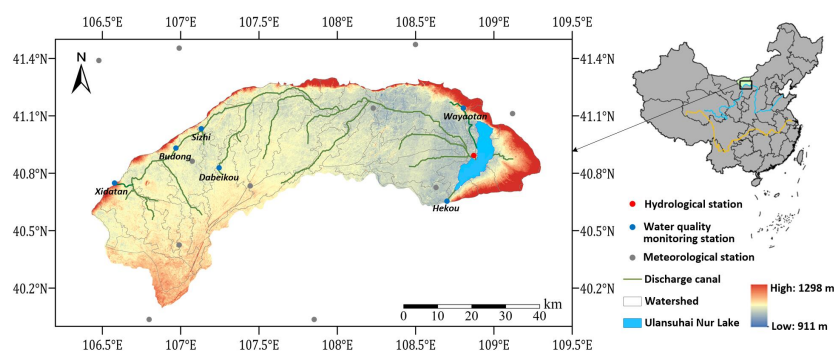


Figure 1. Location of the Hetao area.

2.2. Research Ideas

Precipitation and temperature are the main elements of climate change considered [3] in this paper. It is assumed that future point source emissions, withdrawn water, dam scheduling, cultivated land areas and irrigation systems, etc. are maintained at the current level. The assessment of the impacts of precipitation and temperature changes on DFAA in the Hetao area as follows (Figure 2):

- (1) Changes in precipitation and temperature cause changes in the runoff process [9], thereby exerting direct impact on the temporal and spatial distribution and frequency of future DFAA. This section is based on the RCPs climate scenarios, aiming to estimate future precipitation and temperature in the Hetao area. LDFAI and SDFAI were calculated by using the future precipitation of the Hetao area.
- (2) DFAA and its typical spatial distribution are prone to cause sudden major water pollution in the Ulansuhai Nur Lake [17,20]. We can predict the locations and time of potential DFAA in the future and respond to possible extreme DFAA in advance. This part of assessment used the established distributed water quantity and quality coupling model and future precipitation and temperature data to simulate and analyze the spatial and temporal changes in the water quantity and quality in the Ulansuhai Nur Lake inlet. The probability of joint distribution of DFAA and water quality in the lake inlet was constructed through the Copula function to estimate the probability of sudden water pollution in future DFAA scenarios.

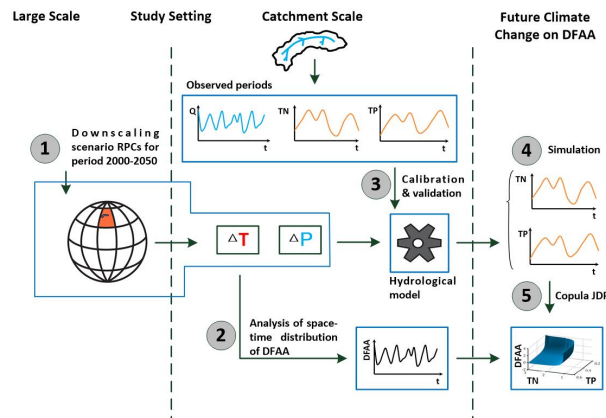


Figure 2. The framework of the impact evaluation of climate change on DFAA and water quality: (1) Selection of climate scenario and derivation of meteorological time series for future climate conditions, (2) Analysis of the spatial and temporal changes of DFAA, (3) Calibration and validation of a hydrological model, (4) Simulate TN and TP data from 1961 to 2050, (5) Calculate multivariate JPD of DFAA, TN and TP.

2.3. Evaluation Indicators

2.3.1. DFAA Indexes

To conduct a quantitative study on the scientific content and basic characteristics of summer LDFAI, researchers defined LDFAI as [19,20]:

$$LDFAI = (P_N - P_P) \times (|P_P| + |P_N|) \times 1.8^{-|P_P+P_N|} \tag{1}$$

where the time scale for calculating the LDFAI is defined as one year; P_P is the pre-flood standard precipitation; P_N is the post-flood standard precipitation; $(P_N - P_P)$ is the DFAA intensity term; $(|P_P| + |P_N|)$ is the drought and flood intensity term; $1.8^{-|P_P+P_N|}$ is the weight coefficient, of which the function is to increase the weight of long cycle DFAA and reduce the weight of pure drought or flood. The standard deviation of precipitation anomalies greater than 0.5 is considered flood, greater than 1 is significant flood, less than -0.5 is drought, less than -1 is significant drought; and between -0.5 and 0.5 is normal precipitation [17]. Based on the hydrometeorological characteristics of the middle and lower reaches of the Yangtze River, in this study the time scale for calculating the LDFAI is defined as two months, i.e., May and June (pre-flood period) and July and August (post-flood period). The long cycle DFAA is judged as LDFAI greater than 1 is a drought-to-flood incident, less than -1 is a flood-to-drought incident, and between -1 and 1 is normal. The greater the absolute value of LDFAI, the more serious the DFAA is.

The SDFAI [19,20] is essentially consistent with the LDFAI, which is expressed as:

$$SDFAI = (P_j - P_i) \times (|P_i| + |P_j|) \times 3.2^{-|P_i+P_j|} \tag{2}$$

where the time scale for calculating the SDFAI is defined as one month; P_i is the pre-flood standard precipitation; P_j is the post-flood standard precipitation. $3.2^{-|P_i+P_j|}$ is the weight coefficient; $j = i + 1 (i = 5, 6, 7, 8, 9)$. The short cycle DFAA is judged as: SDFAI greater than 1 is a drought-to-flood incident, that less than -1 is a flood-to-drought incident and that between -1 and 1 is normal. The greater the absolute value of SDFAI, the more serious the DFAA incident is.

2.3.2. Evaluation of the Relationship between DFAA and Water Quality

Copula is a joint distribution function in a uniform distribution over the interval $[0,1]$ [29,30]. Given F is an n -dimensional distribution function, and the edge distribution of each variable is

F_1, F_2, \dots, F_n , then there is an n -dimensional Copulas function C . For any $x \in R_n$, the distribution function satisfies:

$$F(x_1, x_2, \dots, x_n) = (X_1 \leq x_1, X_2 \leq x_2, \dots, X_n \leq x_n) = C[F_1(x_1), F_2(x_2), \dots, F_n(x_n)] \quad (3)$$

where x_1, x_2, \dots, x_n are the observed samples, and $F(x)$ is the edge distribution function. Three Archimedean Copulas functions were selected, Gumbel-Hougaard (GH), Clayton and Frank, for joint distribution of two-dimensional and three-dimensional DFAA. The parameter estimation of the Copulas function was conducted by the appropriate line method, and the optimal Copula function was selected by a fit test to analyze the relationship between the DFAA and water quality.

With the constructed multivariate joint probability distribution (JPD) of DFAA, TN and TP, two DFAA situations under different water quality conditions in the Hetao area can be analysed:

(1) For future severe DFAA events, the joint transcendence probability is given more attention [31], and the joint probability analysis of TN, the most typical pollutant in the Hetao area, and DFAA, was selected. The multivariate JPD under this condition is denoted as $G_{X,Z}(x, z)$ and can be written as:

$$G_{X,Z}(x, z) = P_{X,Z}(X > x, Z > z) = 1 - F_X(x) - F_Z(z) + C(F_X(x), F_Z(z)) \quad (4)$$

$$G_{X,Z}(x, z) = P_{X,Z}(X > x, Z < z) = F_Z(z) - C(F_X(x), F_Z(z)) \quad (5)$$

where X denotes TN and x is its specific value, Z denotes DFAA and z is its specific value, $G_{X,Z}(x, z)$ is the bivariate JPD of pair (TN, DFAA), $F_X(x)$, $F_Z(z)$ are the marginal distribution function of TN, DFAA, respectively.

(2) When TN and TP exceed a specific value, DFAA is less than or more than a specific value, which addresses the water pollution risk under the DFAA condition. The multivariate JPD under this condition is denoted as $G_{X,Y,Z}(x, y, z)$ and presented as:

$$\begin{aligned} G_{X,Y,Z}(x, y, z) &= P_{X,Y,Z}(X > x, Y > y, Z > z) \\ &= 1 - F_X(x) - F_Y(y) - F_Z(z) + C(F_X(x), F_Y(y)) + C(F_X(x), F_Z(z)) \\ &\quad + C(F_Y(y), F_Z(z)) - C(F_X(x), F_Y(y), F_Z(z)) \end{aligned} \quad (6)$$

$$\begin{aligned} G_{X,Y,Z}(x, y, z) &= P_{X,Y,Z}(X > x, Y > y, Z < z) \\ &= F_Z(z) - C(F_X(x), F_Z(z)) - C(F_Y(y), F_Z(z)) + C(F_X(x), F_Y(y), F_Z(z)) \end{aligned} \quad (7)$$

where X denotes TN and x is its specific value; Y denotes TP and y is its specific value; Z denotes DFAA and z is its specific value; $G_{X,Y,Z}(x, y, z)$ represents the trivariate JPD of pair (TN, TP, DFAA); $F_X(x)$, $F_Y(y)$, and $F_Z(z)$ are the marginal distribution functions of TN, TP and DFAA, respectively.

2.4. Data Collection and Arrangement

The assessment of DFAA in the Hetao area requires data such as geographic information (GIS), monitoring data of meteorology, hydrology and environment [32]. GIS data include digital elevation models (DEM), water systems, vegetation maps, soil maps, meteorological sites, sewage outlets, runoff, and water quality sites distribution; the meteorological data include the sequence of meteorological elements such as historical daily precipitation and the maximum and minimum temperature of each site, and precipitation and temperature data under different meteorological elements of the Global Climate Model (GCM) in the future; the hydrological and water environment data include information such as monitoring section runoff, water quality concentration, and point source discharge. The basic data are shown in Table 1.

Table 1. The database of the climate change impact assessment in the Hetao area.

Type	Data	Scale	Source
GIS	DEM	Grid (90 m × 90 m)	Institute of Geographic Sciences and Natural Resources Research
	Land use	1:1,000,000	Institute of Geographic Sciences and Natural Resources Research
	Agrotype	1:4,000,000	Institute of Geographic Sciences and Natural Resources Research
Meteorology	Meteorological station	11 stations (1961–2017)	China Meteorological Administration
Hydrology	GCM	Grid (1 × 1 °C) (2001–2050)	IPCC Fifth Assessment Report
	Hydrological station	1 station (1980–2000)	Hetao Irrigation Administration Bureau
	Water quality station	6 stations (2012–2015)	Hetao Irrigation Administration Bureau

(1) The RCPs climate scenario

Due to space limitations, the RCPs climate scenario was selected to output precipitation and temperature series, and the 2001 to 2017 rate was periodically divided, and 2018 to 2050 was the forecast period. The precipitation and temperature were statistically analyzed and simulated in the RCP 2.6, RCP 4.5 and RCP 8.5 (as 1, 2 and 3) scenarios through the calibrated and down-scaled GFDL-ESM2M, HadGEM2-ES, IPSL-CM5A-LR, MIROC-ESM-CHEM, and NorESM1-M models (as a, b, c, d and e) from 2001 to 2017 [33]. If the data has uncertainty in the time of acquisition, or the time precision of the data is not met, then the validity of the spatio-temporal data cannot be explained, and reasonable reasoning cannot be made for the uncertain data in the data. Therefore, it is necessary check the uncertainty of the data. For the description of the difference between the RCPs climate scenario, the current mainstream international adopts the Taylor chart method, which is a way to integrate the three indicators of standard deviation (Std), root mean square error (RMSE) and correlation coefficient (R^2) into a concentrated display. The 15 climate models are represented by Taylor diagram and the results are shown in Figure 3. The results were compared with the measured values. HadGEM2-ES in the RCP 8.5 scenario had minimum uncertainty and relatively good precipitation and temperature results, and the correlation coefficients were 0.805 and 0.753, respectively. The results show that the climate model has the lowest uncertainty in all models, accurately simulating historical precipitation changes, and can be used for future precipitation prediction.

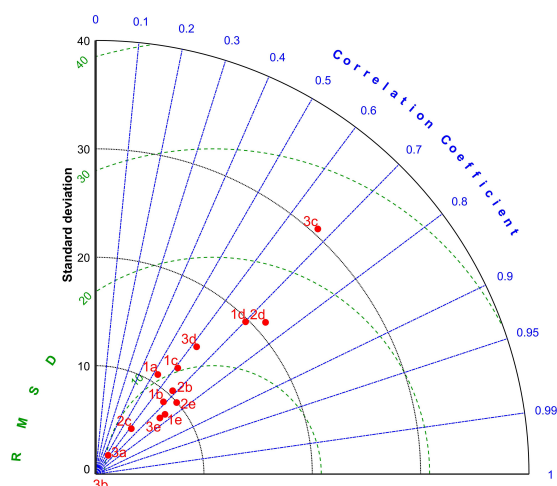


Figure 3. RPC 2.6, 4.5 and 8.4 scenario 15 models of Hetao area annual precipitation estimate Taylor diagram.

In the RCP 8.5 scenario, precipitation and temperature in the Hetao area showed a consistent increase, and compared with the period from 1961 to 2017, the RCP 8.5 scenario showed that precipitation increased by 12.2 mm and the temperature increased by 1.9 °C. When only considering the temperature increase, the frequency and intensity of the drought in the Hetao area will increase in the future; when merely considering the concentrated and increased precipitation, the runoff in the basin will increase, and the flood frequency will increase. The risk of drought and flood caused by climate change will directly affect the yield of local wheat and other crops. Therefore, it is necessary to study the law of DFAA in the area.

(2) Calibration and validation of SWAT Model

The distributed coupling model of water quantity and water quality was developed by Dr. Jeff Arnold in 1998, that is, the watershed integrated management SWAT model [32]. The SWAT model can simulate the influence of climate change on runoff and water quality by changing the input data for scenario design and analysis [34,35]. Because of the large area of plain area, the traditional sub-basin division based on DEM has some difficulties. Based on this, the pre-defined tool of SWAT model is used to quantitatively simulate the water balance and water cycle characteristics of Hetao Irrigation Area under the influence of natural and human activities on the basis of artificially defined river course and sub-basin boundary. The SWAT model parameter calibration period of this study is from 1980 to 1997, and the inspection period is from 1980 to 1997 in this study, and the validation period is from 1998 to 2000. However, due to the limitation of water quality data and measured water quality data, only the monthly concentration data of six stations from 2012 to 2015 were selected to determine the relevant model water quality parameters. When the model structure and input parameters are preliminarily determined, it is necessary to calibrate and verify the model. In this paper, two indicators were selected to evaluate the applicability of the model, the model efficiency coefficient *Ens* proposed by Nash-Sutcliffe [36] and the correlation coefficient R^2 [34]. The Latin hypercube sampling and one-factor-at-a-time (LHS-OAT) method was used to analyze the sensitivity of the parameters. According to the model requirements, when $R^2 \geq 0.6$ and $Ens \geq 0.45$, the simulation results are acceptable. The results of the runoff parameter rate are shown in Table 2. It can be seen from Table 2 that the SWAT model reached the basic evaluation criteria of R^2 and *Ens* for the simulation results of the total drainage flow and the simulation results of each water quality station. Therefore, the SWAT model is applicable to the simulation of flow and water quality in the Hetao area. The precipitation and temperature data from 1961 to 2050 were input into the SWAT model, which simulated the flow and water quality changes in future climate change scenarios, and then the impact of future climate change on DFAA can be studied.

Table 2. Evaluation of the simulation results of monthly TN and TP during calibration and validation periods.

Station	Variety	Calibration		Validation	
		R^2	<i>Ens</i>	R^2	<i>Ens</i>
Zongpaigan	Runoff	0.69	0.61	0.73	0.63
Xidatan	TN	0.8	0.74	0.46	0.45
	TP	0.69	0.68	0.62	0.51
Wayaoatan	TN	0.79	0.77	0.79	0.7
	TP	0.76	0.74	0.81	0.67
Budong	TN	0.72	0.67	0.89	0.46
	TP	0.68	0.57	0.73	0.57

Table 2. Cont.

Station	Variety	Calibration		Validation	
		R ²	Ens	R ²	Enst
Dabeikou	TN	0.71	0.56	0.75	0.51
	TP	0.81	0.56	0.62	0.52
Hekou	TN	0.62	0.51	0.71	0.48
	TP	0.73	0.53	0.67	0.58
Sizhi	TN	0.73	0.61	0.63	0.52
	TP	0.62	0.49	0.65	0.54

3. Results

3.1. Law Analysis of DFAA

3.1.1. Analysis of DFAA on the Time Scale

On the time scale, we compared the trend of the long-term sequence DFAA rather than the characteristics in changes within a year. Therefore, we selected LDFAI for the time-scale analysis of DFAA. The precipitation from 1961 to 2050 was standardized as Equation (1). As shown in Figure 4a, there may be a multiple-level time scale structure and localization characteristics of changes in DFAA in the time domain. Wavelet analysis with the time-frequency multi-resolution function proposed by Morlet provides the possibility of effectively studying the problems of time series, which can clearly reveal multiple change cycles hidden in the time series [37].

The Morlet wavelet analysis of the LDFAI from 1961 to 2050 was conducted to reveal the DFAA cycle in the Hetao area over the past 57 years and predict the change law from 2018 to 2050. The wavelet variance in Figure 4b can reflect the distribution of the wave energy of the LDFAI with time scale, and determine the main cycle during DFAA. There are four distinct peaks in Figure 4b, 3, 6, 11 and 21a, indicating that the quasi-cycles of these four scales play a major role in the DFAA in the Hetao area [37]. The largest peak corresponds to the characteristic time scale of 21a, indicating that it has the strongest periodic turbulence in the most significant cycle, which is the first main cycle of drought and flood changes in the area. The second, third and fourth main cycles of drought and flood changes are 11, 6 and 3a, respectively, representing the following: 21a characteristic time scale has approximately 7 cycles of drought and flood alternation; the average cycle of drought and flood changes is approximately 13a; the drought and flood centers are in 1966, 1980, 1997, 2010, 2022, 2035, 2050; on the 25a characteristic time scale, there are approximately 4 cycles of drought and flood alternation; the average change cycle is approximately 16a; on the 11a characteristic time scale, there are approximately 10 cycles of drought and flood alternation; and the average change cycle is approximately 9a. Regardless of the time scale, the square of modulus of the wavelet coefficient after 2017 has shown a weakening trend, indicating that DFAAs in the Hetao area will decrease in the future. The red (blue) rendering in Figure 4c refers to that where the real part of the wavelet coefficient is positive (negative), and the darker the color is, the greater the degree of the drought or flood. The square of modulus of the wavelet coefficient in Figure 4d refers to the wavelet energy spectrum, and the larger the value (the darker the red), the stronger the wave energy is, and the more significant the cycle is. The two most energy-concentrated centers in Figure 4d represent the characteristics of the changes in wave energy. They are (1) scale of 22 to 26a, wave energy is from the late 1970s to early 1990s, and (2) scale of 19a, the wave energy is the strongest and runs through 2000 to 2025, with the strongest performance.

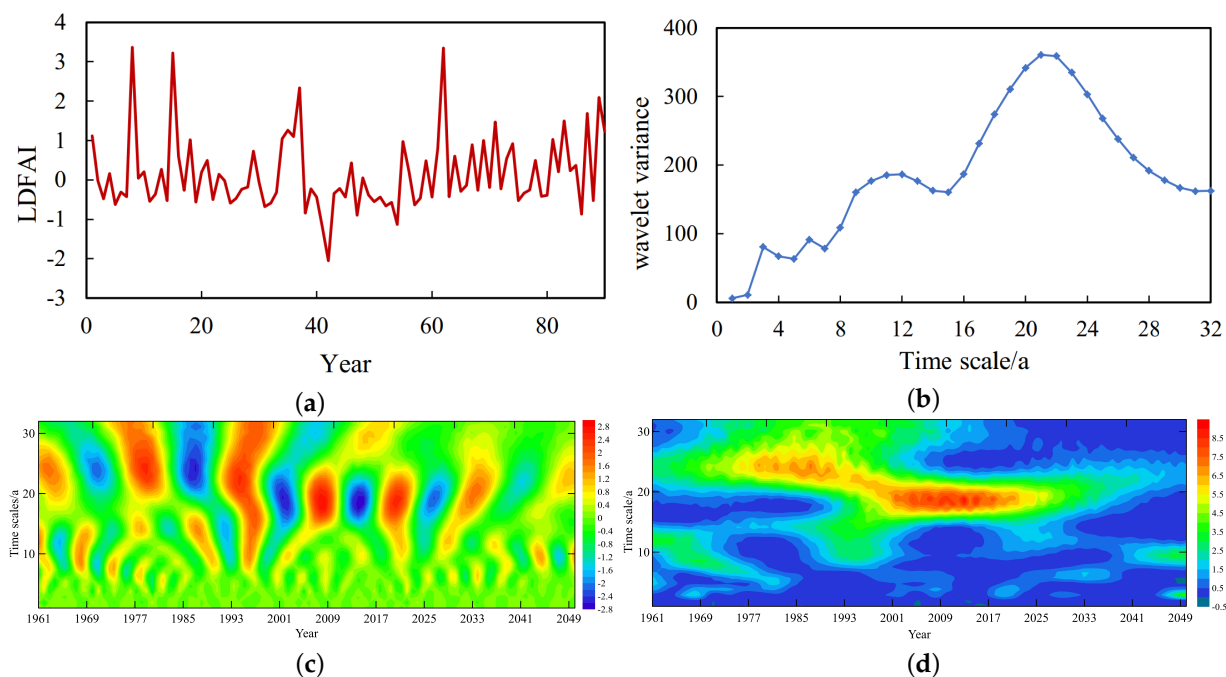


Figure 4. Morlet wavelet analysis of DFAA in the Hetao area during 1961 to 2050. (a) LDFAI; (b) Wavelet variance map; (c) Real part of wavelet transform coefficients; (d) Square of modulus of wavelet transform coefficients.

3.1.2. Analysis of Spatial Differentiation Characteristics of DFAA

On the spatial scale, we pay attention to the spatial position of DFAA occurrence in different months. Therefore, we select SDFAI for the spatial-scale analysis of DFAA (Equation (2)). The spatial distribution of the frequency of DFAA in 11 hydrological stations of the Hetao area from May to July and from July to September are shown in Figure 5. Generally, the precipitation in the Hetao area from July to September is greater than that from May to July, thus the frequency of DFAA in the Hetao area is also reversed; from May to July, the drought-to-flood incidents are frequent, and from July to September, the flood-to-drought incidents are frequent. The spatial distribution of the frequency of DFAA in the Hetao area is uneven, and generally, there is no consistency between drought-to-flood incidents and flood-to-drought incidents in the same period. That is, it is difficult to form short-cycle drought-to-flood-to-drought and flood-to-drought-to-flood incidents in the Hetao area. During the 57 years from 1961 to 2017, the high-frequency DFAA region in the Hetao area is generally concentrated in the east, thereby Ulansuhai Nur Lake has become the most frequent DFAA area, which is unfavourable for maintaining the ecological stability of the lake. However, there are few DFAA in the northern part of the Hetao area. The reason is that the precipitation in the area is relatively balanced from April to September, so DFAA is not frequent. However, from 2018 to 2050, the SDFAI in the Hetao area showed a significant decrease compared with the previous period, which is completely consistent with the previous results of the LDFAI, and the frequent occurrence area has shifted westward.

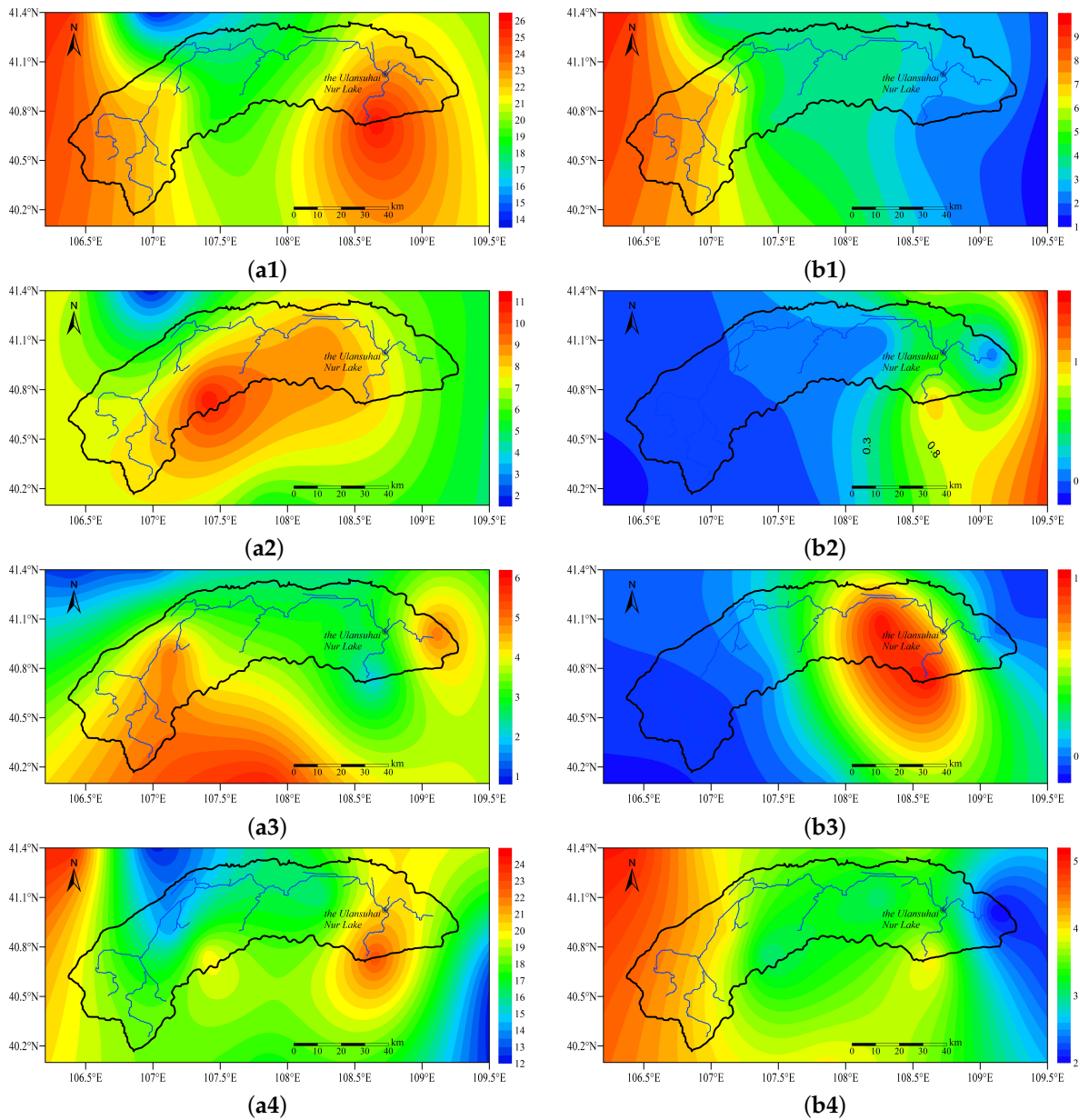


Figure 5. Spatial distribution of the frequency of flood-drought abrupt alternation events in the Hetao Area. (a1) Flood-to-drought from May to July in 1961–2017; (b1) Flood-to-drought from May to July in 2018–2050; (a2) Drought-to-flood from May to July in 1961–2017; (b2) Drought-to-flood from May to July in 2018–2050; (a3) Flood-to-drought from July to September in 1961–2017; (b3) Flood-to-drought from July to September in 2018–2050; (a4) Drought-to-flood from July to September in 1961–2017; (b4) Drought-to-flood from July to September in 2018–2050.

3.2. The Relationship between DFAA and Water Quality

The contour plots of different periods of $G_{X,Z}(x, z)$ are given in Figure 6 (Equation (4) and (5)). They represent the JPD of changes in water quality in past and future natural precipitation conditions, so the joint probability with various given combinations of pair (TN, SDFAI) with a given certain joint probability can be obtained [29–31]. It can be seen from Figure 6 that the value of JPD which exceeds a certain probability becomes larger with more TN and high SDFAI. When $G_{X,Z}(x, z)$ is between 0.1 to 0.3 or 0.8 to 0.9, the contour plot spacing is larger and TN and SDFAI change more obviously compared with that between 0.3 and 0.8. It can be seen from Figure 6 that when the joint distribution probability is determined, we can also compare the TN overshoot probability corresponding to different SDFAI

values. For example, when the joint distribution probability is 0.1 and the SDFAI value exceeds 1.5, the TN value corresponding to Figure 6a is greater than 1.92 mg/L, and the corresponding TN value of Figure 6b is greater than 2.11 mg/L. This result indicates that in future climate change scenarios, when DFAA occurs sharply, the probability of water quality exceeding the standard will increase. The possibility of constructing different combinations of events through conditional probability is listed in Table 3. Between 1961 and 2017, when a drought-to-flood event occurs ($SDFAI > 1$), the probability of TN pollutants exceeding Class III is 0.608; when a flood-to-drought occurs ($SDFAI < -1$), the probability of TN pollutants exceeding Class III is 0.732; when there is no flood-to-drought or drought-to-flood event ($-1 \leq SDFAI \leq 1$), the probability of TN pollutants exceeding Class III is 0.595. Between 2018 and 2050, when a drought-to-flood event occurs ($SDFAI > 1$), the probability of TN pollutants exceeding Class III is 0.712; when a flood-to-drought event occurs ($SDFAI < -1$), the probability of TN pollutants exceeding Class III is 0.797; when there is no flood-to-drought or drought-to-flood event ($-1 \leq SDFAI \leq 1$), the probability of TN pollutants exceeding Class III is 0.432. This result indicates that when DFAA occurs, the probability of TN pollutants in the Ulansuhai Nur Lake entrance is lower than usual, and the probability of TN pollutants accompanying DFAA will increase in the future.

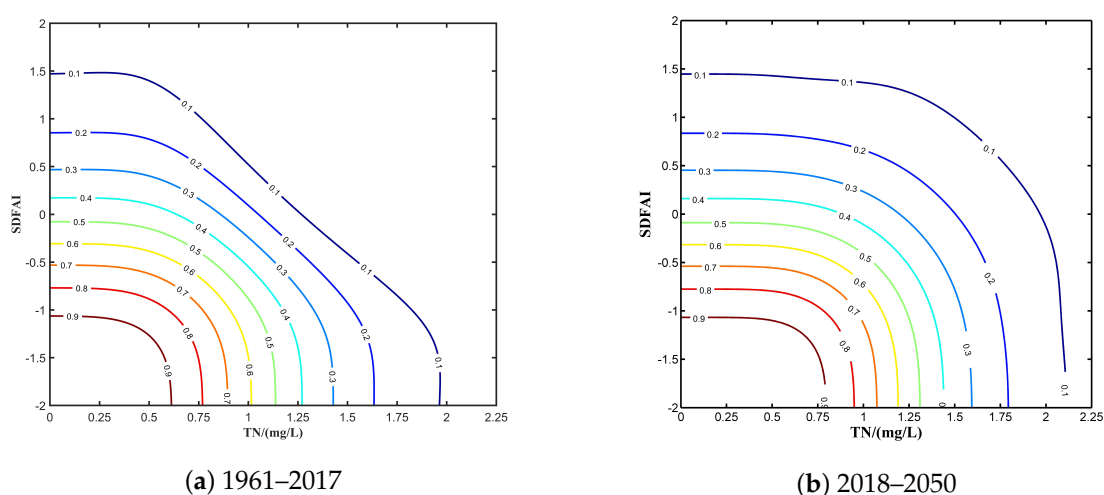


Figure 6. The contour plot of bivariate JPD of TN and SDFAI.

Table 3. The possibility of different bivariate combination events.

Year	$P(TN > 1 \mid SDFAI > 1)$	$P(TN > 1 \mid SDFAI < -1)$	$P(TN > 1 \mid -1 \leq SDFAI \leq 1)$
1961–2017	0.576	0.732	0.578
2018–2050	0.712	0.797	0.432

The contour surface of $G_{X,Y,Z}(x, y, z)$ is shown in Figure 7 (Equations (6) and (7)), which indicates that close dependent correlation exists in TN, TP and SDFAI. Figure 7 expounds the JPD of changes in water quality in past and future natural precipitation conditions, thus the joint probability with various given combinations of pair (TN, TP, SDFAI) as well as the various combinations of pair (TN, TP, SDFAI) with a given certain joint probability can be achieved [29–31]. It can be seen from Figure 7 that the value of JPD which does not exceed a certain probability tends to be large with small TN and TP and low SDFAI. When $G_{X,Y,Z}(x, y, z)$ is between 0.7 to 0.9, the contour surface spacing is larger and TN and TP change more obviously compared with that between 0.1 and 0.7. Similarly, different three-variable event combinations are constructed by conditional probabilities, as shown in Table 4. Between 1961 and 2017, when a drought-to-flood event occurs ($SDFAI > 1$), the probability of one pollutant exceeding the standard or two pollutants exceeding the standard at the same time is 0.939; when a flood-to-drought event occurs ($SDFAI < -1$), the probability of one pollutant exceeding the standard or both pollutants exceeding the standard at the same time is 0.827; when there is no

flood-to-drought or drought-to-flood event ($-1 \leq \text{SDFAI} \leq 1$), the probability is 0.346. Between 2018 and 2050, when a drought-to-flood event occurs ($\text{SDFAI} > 1$), the probability of one pollutant exceeding the standard or two pollutants exceeding the standard at the same time is 0.956; when a flood-to-drought event occurs ($\text{SDFAI} < -1$), the probability of one pollutant exceeding the standard or both pollutants exceeding the standard at the same time is 0.851; when there is no flood-to-drought or drought-to-flood event ($-1 \leq \text{SDFAI} \leq 1$), the probability is 0.336. This result further confirms the results of the bivariate joint distribution. Moreover, the probability of water quality exceeding the standard caused by drought-to-flood events in the joint distribution of three variables is greater than that in flood-to-drought events. Therefore, DFAA and the risk of water pollution in the Hetao area can be clarified more reasonably by using trivariate JPD, and it also provides technological guidance for irrigation planning and DFAA resistance.

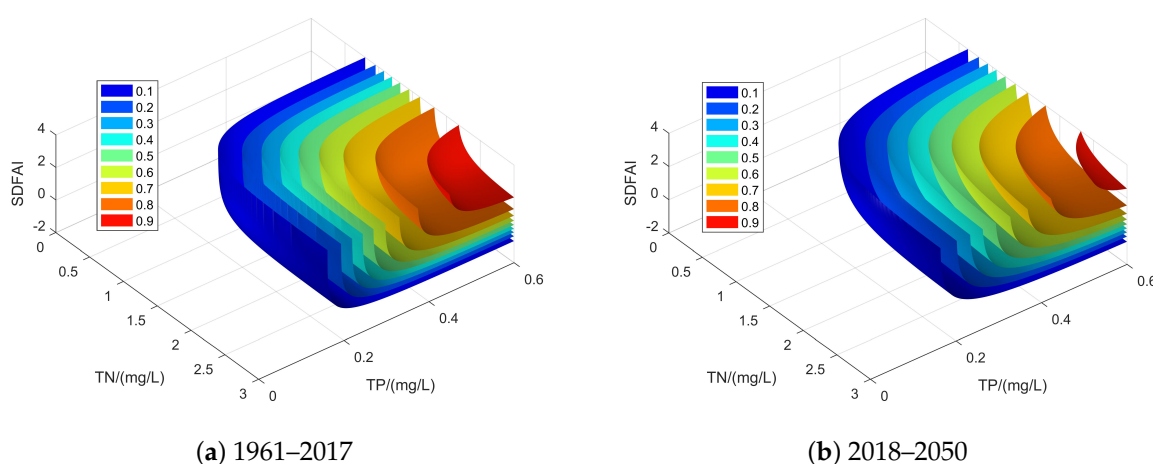


Figure 7. Joint transcendental probability section diagram.

Table 4. The possibility of different trivariate combination events.

Year	$P(A^* \text{SDFAI} > 1)$	$P(A^* \text{SDFAI} < -1)$	$P(B^* -1 \leq \text{SDFAI} \leq 1)$
1961–2017	0.94	0.827	0.346
2018–2050	0.958	0.851	0.336

A*: One pollutant exceeds the standard or two pollutants exceeded the standard simultaneously;
 B*: Two pollutants do not exceed the standard simultaneously.

4. Discussion

The increase in the evaporation rate caused by climate warming resulted in the decrease in available water and the increase in drought events in the mid-latitudes and semi-arid low latitudes [38]. In the future, the increase in temperature and extreme precipitation will aggravate water pollution and accelerate the occurrence of eutrophication events [4,5,39]. These results can also be found in the IPCC report [40]. We believe that under the premise of the reduction in DFAA events in the Hetao area, there are three reasons for the increasing water pollution risk:

- (1) With the increase in precipitation processes, rainwater and runoff pass through the ground, and the pollutants accumulated on the surface are carried into the water body, causing pollution of surface water and even groundwater within the drainage area, especially in the vicinity of farmland or industrial land, which will form serious non-point source pollution [41]. Therefore, the change in precipitation intensity and frequency will affect non-point source pollution. As two of the main elements of non-point source pollution, nitrogen and phosphorus are greatly affected by precipitation process. If precipitation and its strength increase, then the runoff scouring effect will intensify, and the nitrogen and phosphorus loads flowing into the water body will increase accordingly [42].

- (2) With the increase in air temperature, the water surface temperature will also increase, which leads to an increase in the temperature difference and thermocline in the upper and lower layers of water. The presence of thermoclines can lead to the formation of anoxic layers at the bottom of water bodies such as rivers or lakes. Nitrogen and phosphorus release easily from sediment to bottom water in an anoxic bottom water environment, and lead to an increase in nitrogen and phosphorus concentrations in surface water, which is the main reason that nitrogen and phosphorus loads increase with surface runoff coming into the water environment. The increase in water temperature will also increase the activities of microorganisms and promote the release of endogenous nitrogen and phosphorus in sediment. If the nitrogen concentration in the water reaches a certain level, eutrophication will be intensified when environmental conditions such as temperature and light are satisfied [43].
- (3) Under drought conditions, runoff is reduced and the water temperature is relatively high, which will increase the concentration of NH_4^+ and NO_2^- in the water. Some studies have shown that concentrations of NH_4^+ and NO_2^- increased by 1.9 and 1.3 times, respectively, in a dry year and a normal year [44]. The increasing frequency of DFAA will cause a large number of surface pollutants to enter water bodies. Drought-to-flood incidents were taken as an example: in the early stage of drought, the flow rate of the river channel decreased, leading to a decrease in the ability to dilute and transport substances and an increase in the concentration of pollutants in the water body and surrounding farmlands. In the later stage of rapid formation of flood, the hydrodynamic conditions increased rapidly, directly bringing a multitude of pollutants in the surrounding farmlands and the river channel into the Ulansuhai Nur Lake. These processes may occur simultaneously with DFAA. At the same time, DFAA will also cause a large amount of sediment to enter water bodies or cause sediment resuspension, which will affect the sediment content of the water body, thus further affecting the transport and transformation of pollutants, and water quality [45,46].

5. Conclusions

According to daily precipitation data from 1961 to 2050 in the Hetao area, monthly TN and TP data, and LDFAI and SDFAI analysis, this paper comprehensively analyzed changes in the DFAA trend in the Hetao area, the spatial and temporal distribution characteristics and the risk of water pollution caused by DFAA. The main conclusions are as follows:

- (1) In the Hetao area, the phenomenon of the LDFAI was mainly for drought-to-flood events, and there is a trend that the frequency of DFAA will decrease in the future; the drought-to-flood incidents occurred frequently in May to July among the SDFAI, and flood-to-drought incidents occurred frequently from July to September.
- (2) Due to the uneven distribution of precipitation in the flood season in the Hetao area, the spatial distribution of the DFAA is not uniform; during the 57 years from 1961 to 2017, the high-frequency DFAA regions in the Hetao area were generally concentrated in the Ulansuhai Nur Lake in the eastern part of the region. From 2018 to 2050, frequent occurrences of DFAA occurred in the west.
- (3) The Copula function is used to calculate the JDP of SDFAI, TN and TP. The risk of water quality exceeding the standard will increase when the DFAA happens, and the probability of water quality exceeding the standard caused by drought-to-flood in the three variable joint distribution is greater than that in flood-to-drought.
- (4) Extreme weather such as an increase in future temperatures and an increase in extreme precipitation will exacerbate water pollution, causing further increases in the risk of excessive water quality in future DFAA, which is consistent with the conclusions of the IPCC report. The results can provide a basis for flood control and drought resistance and pollution control in the Hetao area.

Author Contributions: This study was designed by Y.Y. and B.W., W.B. and T.X. contributed to data collection and calculation. Y.Y. carried out calculation analysis and completed the manuscript. D.Y. and J.M. contributed to the manuscript modification.

Funding: This research was funded by the National Key Research and Development Project (No. 2016YF - A0601503), the National Natural Science Foundation of China (No. 91547209), the National Key Research and Development Project (No. 2017YFA0605004), and the Public Service Special Project of the Environmental Protection Ministry of China (No. 201509027).

Conflicts of Interest: The authors declare no conflict of interest.

Abbreviations

The following abbreviations are used in this manuscript:

DFAA	Drought-flood abrupt alternation
RCPs	Representative Concentration Pathways
TN	Total nitrogen
TP	Total phosphorus
IPCC	Intergovernmental Panel on Climate Change
DEM	Digital Elevation Model
GCM	Global Climate Model
LDFAI	Long-cycle drought-flood abrupt alternation index
SDFAI	Short-cycle drought-flood abrupt alternation index
JPD	Joint probability distribution

References

1. IPCC. Summary for Policymakers. In *Global Warming of 1.5 °C; An IPCC Special Report on the Impacts of Global Warming of 1.5 °C above Pre-Industrial Levels and Related Global Greenhouse Gas Emission Pathways, In the Context of Strengthening the Global Response to the Threat of Climate Change, Sustainable Development, and Efforts to Eradicate Poverty*; Intergovernmental Panel on Climate Change (IPCC): Geneva, Switzerland, 2018.
2. Walther, G.R.; Post, E.; Convey, P.; Menzel, A.; Parmesan, C.; Beebee, T.J.C.; Fromentin, J.M.; Hoegh-Guldberg, O.; Bairlein, F. Ecological responses to recent climate change. *Nature* **2002**, *416*, 389–395. [[CrossRef](#)] [[PubMed](#)]
3. Rogelj, J.; Meinshausen, M.; Knutti, R. Global warming under old and new scenarios using IPCC climate sensitivity range estimates. *Nat. Clim. Chang.* **2012**, *2*, 248–253. [[CrossRef](#)]
4. Harvell, C.D.; Mitchell, C.E.; Ward, J.R.; Altizer, S.; Dobson, A.P.; Ostfeld, R.S.; Samuel, M.D. Climate warming and disease risks for terrestrial and marine biota. *Science* **2002**, *296*, 58–62. [[CrossRef](#)] [[PubMed](#)]
5. Walter, K.M.; Zimov, S.A.; Chanton, J.P.; Verbyla, D.; Chapin, F.S. Methane bubbling from Siberian thaw lakes as a positive feedback to climate warming. *Nature* **2006**, *443*, 71–75. [[CrossRef](#)] [[PubMed](#)]
6. Parmesan, C.; Yohe, G. A globally coherent fingerprint of climate change impacts across natural systems. *Nature* **2003**, *443*, 37–42. [[CrossRef](#)]
7. Yang, S.Y.; Wu, B.Y.; Zhang, R.H.; Zhou, S.W. Relationship between an abrupt drought-flood transition over mid-low reaches of the Yangtze River in 2011 and the intraseasonal oscillation over mid-high latitudes of East Asia. *Acta Meteorol. Sin.* **2013**, *27*, 129–143. [[CrossRef](#)]
8. Espinoza, J.C.; Ronchail, J.; Guyot, J.L.; Junquas, C.; Drapeau, G.; Martinez, J.M.; Santini, W.; Vauchel, P.; Lavado, W.; Ordonez, J.; et al. From drought to flooding: Understanding the abrupt 2010–11 hydrological annual cycle in the Amazonas River and tributaries. *Environ. Res. Lett.* **2012**, *7*, 1–7. [[CrossRef](#)]
9. Vogel, J.L.; Huff, F.A. Relation Between the St-Louis Urban Precipitation Anomaly and Synoptic Weather Factors. *J. Appl. Meteorol. Clim.* **1978**, *17*, 1141–1152. [[CrossRef](#)]
10. Trenberth, K.E.; Guillemot, C.J. Physical Processes Involved in the 1988 Drought and 1993 Floods in North America. *J. Clim.* **1996**, *9*, 1288–1298. [[CrossRef](#)]
11. Cook, B.I.; Seager, R.; Miller, R.L. Atmospheric circulation anomalies during two persistent north american droughts: 1932–1939 and 1948–1957. *Clim. Dyn.* **2011**, *36*, 2339–2355. [[CrossRef](#)]

12. Garnett, E.R.; Khandekar, M.L. The impact of large-scale atmospheric circulations and anomalies on Indian monsoon droughts and floods and on world grain yields—a statistical analysis. *Agric. For. Meteorol.* **1992**, *61*, 113–128. [[CrossRef](#)]
13. Hastenrath, S.; Polzin, D.; Mutai, C. Diagnosing the droughts and floods in equatorial East Africa during boreal autumn 2005–08. *J. Clim.* **2010**, *23*, 813–817. [[CrossRef](#)]
14. Zhang, Z.Z.; Chao, B.F.; Chen, J.L.; Wilson, C.R. Terrestrial water storage anomalies of Yangtze River Basin droughts observed by GRACE and connections with ENSO. *Glob. Planet. Chang.* **2015**, *126*, 35–45. [[CrossRef](#)]
15. Keyantash, J.; Dracup, J.A. The Quantification of Drought: An Evaluation of Drought Indices. *Am. Meteorol. Soc.* **2002**, *83*, 1167–1180. [[CrossRef](#)]
16. Tote, C.; Patricio, D.; Boogaard, H.; van der Wijngaart, R.; Tarnavsky, E.; Funk, C. Evaluation of Satellite Rainfall Estimates for Drought and Flood Monitoring in Mozambique. *Remote Sens.* **2015**, *7*, 1758–1776. [[CrossRef](#)]
17. Li, X.H.; Zhang, Q.; Zhang, D.; Ye, X.C. Investigation of the drought-flood abrupt alternation of streamflow in Poyang Lake catchment during the last 50 years. *Hydrol. Res.* **2017**, *48*, 1402–1417. [[CrossRef](#)]
18. Gao, C.; Tian, R. The influence of climate change and human activities on runoff in the middle reaches of the Huaihe River Basin, China. *J. Geogr. Sci.* **2018**, *28*, 79–92. [[CrossRef](#)]
19. Wu, Z.W.; Li, J.P.; He, J.H.; Jiang, Z.H. Occurrence of droughts and floods during the normal summer monsoons in the mid and lower reaches of the Yangtze River. *Geophys. Res. Lett.* **2006**, *33*, L05813. [[CrossRef](#)]
20. Wu, Z.W.; Li, J.P.; He, J.H.; Jiang, Z.H. Large-scale atmospheric singularities and summer long-cycle droughts-floods abrupt alternation in the middle and lower reaches of the Yangtze River. *Chin. Sci. Bull.* **2006**, *51*, 2028–2034. [[CrossRef](#)]
21. Mosavi, A.; Ozturk, P.; Chau, K.W. Flood Prediction Using Machine Learning Models: Literature Review. *Water* **2018**, *10*, 1536. [[CrossRef](#)]
22. Mosavi, A.; Edalatfar, M. A Hybrid Neuro-Fuzzy Algorithm for Prediction of Reference Evapotranspiration. In Proceedings of the International Conference on Global Research and Education, Iasi, Romania, 25–28 September 2017; pp. 235–243.
23. Choubin, B.; Moradi, E.; Golshan, M.; Adamowski, J.; Sajedi-Hosseini, F.; Mosavi, A. An ensemble prediction of flood susceptibility using multivariate discriminant analysis, classification and regression trees, and support vector machines. *Sci. Total Environ.* **2019**, *10*, 2087–2096. [[CrossRef](#)] [[PubMed](#)]
24. Yang, C.G.; Yu, Z.B.; Hao, Z.C.; Zhang, J.Y.; Zhu, J.T. Impact of climate change on flood and drought events in Huaihe River Basin, China. *Hydrol. Res.* **2012**, *43*, 14–22. [[CrossRef](#)]
25. Hurlbert, M.; Gupta, J. Adaptive Governance, Uncertainty, and Risk: Policy Framing and Responses to Climate Change, Drought, and Flood. *Risk Anal.* **2016**, *36*, 339–356. [[CrossRef](#)]
26. Zhu, D.N.; Ryan, M.C.; Sun, B.; Li, C.Y. The influence of irrigation and Wuliangshuai Lake on groundwater quality in eastern Hetao Basin, Inner Mongolia, China. *Hydrogeol. J.* **2014**, *22*, 1101–1114. [[CrossRef](#)]
27. Wu, Y.; Shi, X.H.; Li, C.Y.; Zhao, S.N.; Pen, F.; Green, T.R. Simulation of Hydrology and Nutrient Transport in the Hetao Irrigation District, Inner Mongolia, China. *Water* **2017**, *9*, 169. [[CrossRef](#)]
28. Zhang, H.; Ma, D.; Hu, X. Arsenic pollution in groundwater from Hetao Area, China. *Environ. Geol.* **2002**, *41*, 638–643. [[CrossRef](#)]
29. Mou, S.Y.; Shi, P.; Qu, S.M.; Ji, X.M.; Zhao, L.L.; Feng, Y.; Chen, C.; Dong, F.C. Uncertainty Analysis of Two Copula-Based Conditional Regional Design Flood Composition Methods: A Case Study of Huai River, China. *Water* **2018**, *10*, 1872. [[CrossRef](#)]
30. Aranda, J.A.; Garcia-Bartual, R. Synthetic Hydrographs Generation Downstream of a River Junction Using a Copula Approach for Hydrological Risk Assessment in Large Dams. *Water* **2018**, *10*, 1570. [[CrossRef](#)]
31. Cai, W.Y.; Di, H.; Liu, X.P. Estimation of the Spatial Suitability of Winter Tourism Destinations Based on Copula Functions. *Int. J. Environ. Res. Public Health* **2019**, *16*, 186. [[CrossRef](#)]
32. Arnold, J.G.; Moriasi, D.N.; Gassman, P.W.; Abbaspour, K.C.; White, M.J.; Srinivasan, R.; Santhi, C.; Harmel, R.D.; van Griensven, A.; Van Liew, M.W.; et al. Swat: Model Use, Calibration, and Validation. *Trans. Asabe* **2012**, *55*, 1491–1508. [[CrossRef](#)]
33. Nazari-Sharabian, M.; Taheriyoun, M.; Ahmad, S.; Karakouzian, M.; Ahmadi, A. Water Quality Modeling of Mahabad Dam Watershed—Reservoir System under Climate Change Conditions, Using SWAT and System Dynamics. *Water* **2019**, *11*, 394. [[CrossRef](#)]

34. Abbaspour, K.C.; Yang, J.; Maximov, I.; Siber, R.; Bogner, K.; Mieleitner, J.; Zobrist, J.; Srinivasan, R. Modelling hydrology and water quality in the pre-alpine/alpine Thur watershed using SWAT. *J. Hydrol.* **2007**, *333*, 413–430. [[CrossRef](#)]
35. Srinivasan, R.; Ramanarayanan, T.S.; Arnold, J.G.; Bednarz, S.T. Large area hydrologic modeling and assessment—Part II: Model application. *J. Am. Water Resour. Assoc.* **1998****2008**, *34*, 142–149. [[CrossRef](#)]
36. Moriasi, D.N.; Arnold, J.G.; Van Liew, M.W.; Bingner, R.L.; Harmel, R.D.; Veith, T.L. Model Evaluation Guidelines for Systematic Quantification of Accuracy in Watershed Simulations. *Trans. Asabe* **2007**, *50*, 885–900. [[CrossRef](#)]
37. Kovacs, J.; Gaborhatvani, I.; Korponai, J.; Kovacs, I.S. Morlet wavelet and autocorrelation analysis of long-term data series of the Kis-Balaton water protection system (KBWPS). *Ecol. Eng.* **2010**, *36*, 1469–1477. [[CrossRef](#)]
38. Whitehead, P.G.; Wilby, R.L.; Battarbee, R.W.; Kernan, M.; Wade, A.J. A review of the potential impacts of climate change on surface water quality. *Hydrolog. Sci. J.* **2009**, *54*, 101–123. [[CrossRef](#)]
39. Ducharme, A. Importance of stream temperature to climate change impact on water quality. *Hydrol. Earth Syst. Sci.* **2008**, *12*, 797–810. [[CrossRef](#)]
40. Stocker, T.F.; Qin, D.; Plattner, G.K.; Tignor, M.M.B.; Allen, S.K.; Boschung, J.; Nauels, A.; Xia, Y.; Bex, V.; Midgley, P.M. *Climate Change 2013: The Physical Science Basis*; University Press: Cambridge, UK, 2013; pp. 1–33.
41. Kaste, O.; Wright, R.F.; Barkved, L.J.; Bjerkeng, B.; Engen-Skaugen, T.; Magnusson, J.; Saelthun, N.R. Linked models to assess the impacts of climate change on nitrogen in a Norwegian river basin and FJORD system. *Sci. Total Environ.* **2006**, *365*, 1–3. [[CrossRef](#)]
42. Whitehead, P.G.; Butterfield, D.; Wade, A.J. The title of the cited article. *Hydrol. Res.* **2009**, *40*, 113–122. [[CrossRef](#)]
43. Luo, Y.Z.; Ficklin, D.L.; Liu, X.M.; Zhang, M.H. Assessment of climate change impacts on hydrology and water quality with a watershed modeling approach. *Sci. Total Environ.* **2013**, *450*, 72–82. [[CrossRef](#)]
44. Vliet, M.T.H.V.; Zwolsman, J.J.G. Impact of summer droughts on the water quality of the meuse river. *J. Hydrol.* **2008**, *353*, 1–17. [[CrossRef](#)]
45. Breivik, K.; Wania, F.; Muir, D.C.G.; Alaee, M.; Backus, S.; Pacepavicius, G. Empirical and modeling evidence of the long-range atmospheric transport of decabromodiphenyl ether. *Environ. Sci. Technol.* **2006**, *40*, 4612–4618. [[CrossRef](#)] [[PubMed](#)]
46. Hilscherova, K.; Dusek, L.; Kubik, V.; Cupr, P.; Hofman, J.; Klanova, J.; Holoubek, I. Redistribution of organic pollutants in river sediments and alluvial soils related to major floods. *J. Soil Sediment.* **2007**, *7*, 167–177. [[CrossRef](#)]

